

## Toward More Accurate Retrievals of Ice Water Content from Radar Measurements of Clouds

CHUN-LEI LIU AND ANTHONY J. ILLINGWORTH

*Joint Centre for Mesoscale Meteorology, Department of Meteorology, University of Reading, Reading, United Kingdom*

(Manuscript received 3 August 1998, in final form 16 August 1999)

### ABSTRACT

There has been considerable discussion concerning the accuracy of values of ice water content (IWC) in ice clouds derived from measurements of radar reflectivity ( $Z$ ). In this paper, the various published relationships that are based on ice particle size spectra recorded from aircraft are analyzed, and it is shown that a relationship between ice water content and reflectivity can be derived ( $IWC = 0.137Z^{0.64}$  at 94 GHz and  $IWC = 0.097Z^{0.59}$  at 35 GHz), which only varies by 20%–30% for different climatological areas, providing the same ice density as a function of particle size is assumed. Uncertainty as to the true variation of density of ice particles with size may reduce the average IWC for a given  $Z$  by up to 30% for an IWC of  $\approx 0.1 \text{ g m}^{-3}$  and 20% for an IWC of  $\approx 0.01 \text{ g m}^{-3}$ . Individual values of IWC derived from a single measurement of  $Z$  are likely to have an error of about +100% and –50%, but if some characteristic size estimate is available, this is reduced to about +50% and –30%. The remaining errors are due to deviations of the size spectra from exponentiality, so there is no advantage in measuring the characteristic size more precisely than this limit. Remote sensing of ice particle size is not trivial, and it is shown that if instead of size, an estimate of the temperature of the ice cloud to within 6 K is available, then, rather surprisingly, the reduction in the error of IWC is almost as good as that achieved using size. Essentially this result is reflecting the well-known correlation of crystal size with temperature. When the mean values of IWC for a given  $Z$  and  $T$  are compared for a tropical and midlatitude dataset using a common ice density variation with size, then the difference is usually less than 25%. A spaceborne instrument may need to integrate over horizontal distances of 10 km to achieve sufficient sensitivity; this necessity may introduce a bias into the retrieved IWC because the relationship between IWC and  $Z$  is not linear, but analysis shows that any bias should be less than 10%.

### 1. Introduction

Ice clouds play a crucial role in the earth's radiation balance (Stephens et al. 1990). In order to validate their representation in global circulation models used for weather forecasting and climate research there is a requirement to obtain global data on the vertical structure of ice water content (IWC) in clouds. It has been suggested that both ground-based and spaceborne millimeter-wave radar could provide such a dataset. The uncertainty in deriving IWC from radar reflectivity,  $Z$ , arises because  $Z$  depends on  $\sum ND^6$  (where  $N$  is the concentration of ice particles of diameter  $D$ ) with a weighting that depends on the dielectric constant of the ice, but  $IWC = (\pi/6) \sum \rho ND^3$ , where  $\rho$  is the ice density of particles with a diameter  $D$ . Variability in the ice particle size spectra and the density of the ice particles will lead to a range of values of IWC for a given ob-

served  $Z$ . Millimeter-wave radars with frequencies of 94 and 35 GHz are now being used for observing ice particles because of their increased sensitivity, and so the onset of Mie scattering by the larger ice particles can introduce a further uncertainty into the values of  $Z$ .

The errors involved in deriving IWC from  $Z$  for ice clouds have been investigated recently by analyzing extensive datasets of ice particle size spectra obtained by penetrating aircraft, and calculating the values of  $Z$  and IWC from these spectra. For consistency in this paper we shall use the definition of  $Z$  referred to a 1 mm raindrop per cubic meter with a centimeter-wavelength radar; we find this preferable to referring  $Z$  to an ice particle because the definition would then need to assume some property of the ice particle and the radar wavelength. The values of the equivalent radar reflectivity can then be calculated from the ice crystal size spectra using

$$Z = \sum_i |K(\rho)|^2 N(D) D^6 f(D, \rho) / 0.93, \quad (1)$$

where the summation is over all size channels of the measured spectrum. The factor  $K$  is given by

*Corresponding author address:* Dr. Anthony J. Illingworth, Department of Meteorology, University of Reading, Earley Gate, P.O. Box 243, Reading RG6 6BB, United Kingdom.  
E-mail: a.j.illingworth@reading.ac.uk

$$K = \frac{m^2 - 1}{m^2 + 2}, \quad (2)$$

where  $m$  is the complex refractive index of ice for the assumed density for a particle of size  $D$ ,  $f(D, \rho)$  is the ratio of the Mie scattering to the Rayleigh scattering for the frequency, and the factor 0.93 is chosen so that, for water in the Rayleigh region, the expression reduces to  $\Sigma ND^6$ . In addition a shape factor may be needed to account for the presence of nonspherical ice particles, although, as we shall see, this is less important for larger ice particles because of their lower density. We assume that if any supercooled liquid cloud droplets are present then they are smaller than the ice particles and so their contribution to  $Z$  is negligible.

In section 2 of this paper we review the proposed relationships between IWC and  $Z$  based on aircraft measurements of ice particle spectra, and show that the apparent conflicts can be resolved when common assumptions are made. There is still some uncertainty arising from different methods of estimating size from particle images and the choice of relationship between particle size and density. Although there is a consistency between the mean relationships between IWC and  $Z$ , our analysis confirms that the values of IWC derived from an individual  $Z$  measurement have an error of about a factor of 2. In section 3 we explore how this mean relationship is affected by ice particle density assumptions. Brown et al. (1995) suggest that if some independent measurement of mean ice particle size is available, such as might be supplied by coincident lidar observations (Intrieri et al. 1993), then this error in IWC from an individual  $Z$  measurement should be reduced to a factor of +50% and -30%. In section 4 we show that if temperature,  $T$ , rather than mean size, is used in addition to  $Z$  then the error in IWC is reduced to the same level as can be achieved from the size information. The errors using  $Z$  and  $T$  rather than  $Z$  and size are compared in section 5. A spaceborne cloud radar may need to integrate along a horizontal path of up to 10-km length and because IWC is not a linear function of  $Z$  then a bias may be introduced into the IWC estimated by integrating along an inhomogeneous cloud field. This effect is analyzed in section 6.

**2. Proposed relationships between IWC and  $Z$**

Sassen (1987) analyzed data from various sources, many of which were ground observations of precipitating ice particles, and deduced a relationship of the form

$$\text{IWC} = 0.037Z^{0.7}, \quad (3)$$

where IWC is in  $\text{g m}^{-3}$  and  $Z$  is in  $\text{mm}^6 \text{m}^{-3}$ . If we consider observations taken within ice clouds then the spread of published IWC- $Z$  relationships is well illustrated by Fig. 1a, which is taken from Matrosov (1997)

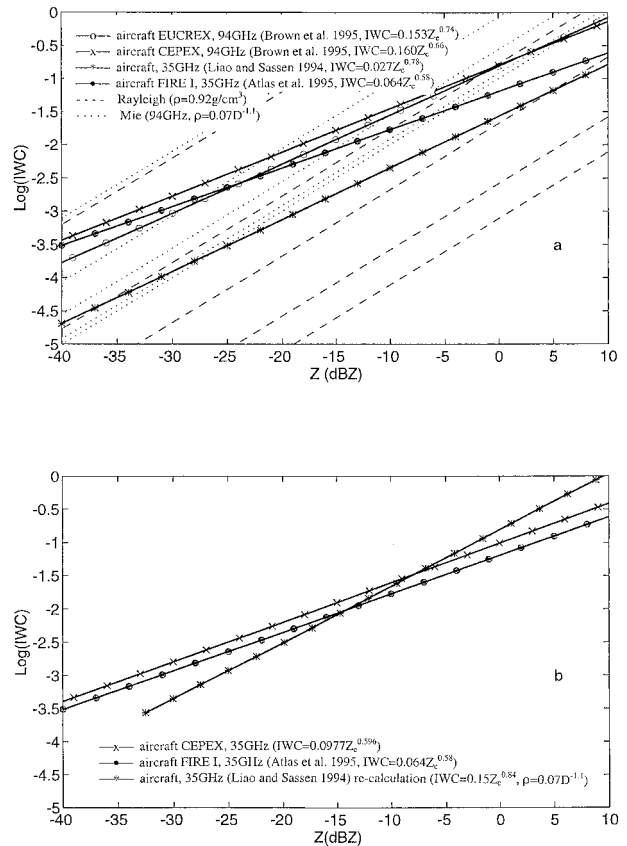


FIG. 1. (a) Proposed IWC- $Z$  relationship derived from ice particle size spectra in cirrus after Matrosov (1997). The solid lines represent mean relationships calculated from aircraft data in three separate field experiments. The dotted and dashed lines represent the theoretical relationships for exponential distributions with different  $D^*$ . The five dashed lines represent solid ice and Rayleigh scattering for  $D^* = 15, 50, 100, 200,$  and  $300 \mu\text{m}$  (left to right). Similarly, the dotted lines represent 94 GHz and variable ice density for  $D^* = 15, 100, 200,$  and  $300 \mu\text{m}$  (left to right). (b) The three curves of aircraft data in (a) replotted for 35 GHz and variable ice density.

and suggests that for a given value of  $Z$  the range of mean IWC predicted can vary by 1.5 orders of magnitude. The data in Fig. 1a are from the CEPLEX (Central Equatorial Pacific Experiment) and EUCREX (European Cirrus and Radiation Experiment) experiments (Brown et al. 1995), the FIRE-I campaign (Atlas et al. 1995) and the ice data obtained in 1973-75 by Heymsfield and Platt (1984) as analyzed by Liao and Sassen (1994). Climatological differences in the average properties of ice clouds will contribute to the scatter in the four solid lines in Fig. 1a, but a major factor arises from different assumptions made in the calculations of  $Z$  and IWC from the ice particle images. Liao and Sassen (1994) assumed that all the ice particles had the density of solid ice, although they did comment that the presence of low density relatively large particles would have a significant effect on radar-reflectivity relationships. Both Atlas et al. (1995) and Brown et al. (1995) used the same ice density versus diameter relationship:

TABLE 1. Theoretical values of  $a$  in  $IWC = aZ$  for exponential ice spectra with various values of  $D^*$  and  $\rho$  (solid ice or  $\rho = 0.07D^{-1.1}$ ).

	W band		Ka band		Rayleigh	
	Solid	$0.07D^{-1.1}$	Solid	$0.07D^{-1.1}$	Solid	$0.07D^{-1.1}$
$D^* = 15$	6.2517	7.8886	6.2373	7.8705	6.2661	7.8886
$D^* = 50$	0.1750	0.8630	0.1690	0.8318	0.1683	0.8260
$D^* = 100$	0.0266	0.2773	0.0215	0.2366	0.0210	0.2307
$D^* = 200$	0.0087	0.1205	0.0029	0.0689	0.0026	0.0618
$D^* = 300$	0.0066	0.1000	0.0011	0.0362	0.0008	0.0285

$$\rho = 0.07D^{-1.1}, \quad (4)$$

(where  $\rho$  is the density in  $\text{g cm}^{-3}$  and  $D$  is in mm), for particles larger than 0.1 mm and the density of solid ice for smaller particles. This is based partly on the mass–size relationships proposed for ice aggregates (e.g., Locatelli and Hobbs 1974) and also on the evidence of Brown and Francis (1995) who compared IWC calculated from ice particle spectra with IWC measured directly by a device that evaporated the ice and then measured the humidity. If solid ice spheres were assumed then the IWC calculated from the spectra exceeded the directly observed value by over a factor of 4. The second difference in the assumptions in Fig. 1a, is that Atlas et al. (1995) and Liao and Sassen (1994) carried out their calculations at 35 GHz whereas those of Brown et al. (1995) were at 94 GHz. If larger particles are present then Mie scattering at 94 GHz will reduce the value of  $Z$  for a given IWC but values at 35 GHz will be less affected.

The effects of the wavelength and density assumptions are also indicated by the broken lines in Fig. 1a. Aircraft measurements of ice particle size spectra in ice clouds show that they are generally of exponential form

$$N(D) = N_0 \exp(-D/D^*), \quad (5)$$

where  $D^* = D_0/3.67$  and  $D_0$  is the median volume diameter. For a constant value of  $D^*$ , IWC is linearly proportional to  $Z$ , so  $b = 1$  in the expression  $IWC = aZ^b$ . The dashed lines in Fig. 1a are theoretical curves for values of  $D^*$  of 15, 50, 100, 200, and 300  $\mu\text{m}$  assuming solid ice and Rayleigh scattering, whereas the dotted lines are for the same range of  $D^*$  but with an ice density given by Eq. (4) and a frequency of 94 GHz so that Mie scattering reduces the  $Z$  values of the larger particles. The effects are quite large: for  $D^* = 300 \mu\text{m}$ , solid ice spheres and Rayleigh scattering, the value of IWC for a given  $Z$  is over a hundred times lower than the IWC for the same  $Z$  observed at 94 GHz and an ice density decreasing with size according to Eq. (4). The effect of Mie scattering and the density variation is to lessen the sensitivity of the IWC– $Z$  relationship to changes in particle size. For example, at 94 GHz and low density ice, changing  $D^*$  from 50 to 300  $\mu\text{m}$  for a constant  $Z$  reduces IWC by a factor of 7, but for solid ice spheres and Rayleigh scattering the reduction is a factor of 210. These sensitivities are summarized in Table 1, which tabulates the value of  $a$  in the expression

$IWC = aZ^b$  for various values of  $D^*$  for 94 GHz, 35 GHz, and Rayleigh scattering and for both solid ice and the density variation of Eq. (4). The values in Table 1 are for a constant  $D^*$  so that the value of  $b$  in  $IWC = aZ^b$  is unity, and  $a$  is the IWC for a  $Z$  of 0 dBZ. The effect of Mie scattering by the larger particles in the spectrum becomes appreciable at 35 GHz for  $D^*$  above 300  $\mu\text{m}$ , but is significant at 94 GHz when  $D^*$  is only 100  $\mu\text{m}$ .

In Fig. 1b the ice cloud relationships in Fig. 1a have been recalculated on the common basis of a 35-GHz frequency and the same variable ice density of Eq. (4). Recomputing the CEPEX data now shows a much closer agreement with the Atlas et al. data; the exponent is virtually identical, but values of IWC for a given  $Z$  from FIRE-I are about 30% lower than those from CEPEX. Recomputing the Liao and Sassen curve was more complicated as we did not have access to the original data. Instead we assumed that the original spectra were exponential, and then calculated the values of  $N_0$  and  $D_0$  corresponding to 35 GHz and solid ice from lines similar to those in Fig. 1a, and then computed the new values of IWC and  $Z$  when the variable ice density was used. The effect is to reduce both  $Z$  and IWC for each point on the line, but the reduction in  $Z$  is larger. The original Liao and Sassen computed reflectivities extended down to values of  $-20$  dBZ, but for the new density, this is lowered to  $-32$  dBZ. In view of the assumption involved, the agreement with the recomputed Liao and Sassen curve in Fig. 1b is surprisingly good, particularly over the range of IWC from 0.1 to 0.001  $\text{g m}^{-3}$ . We conclude that the independent datasets of ice particle spectra lead to a consistent mean relationship between IWC and  $Z$ :

$$IWC = 0.137Z^{0.643} \quad \text{at 94 GHz} \quad \text{and} \quad (6a)$$

$$IWC = 0.097Z^{0.59} \quad \text{at 35 GHz}, \quad (6b)$$

providing the same ice density–size variation is used. These equations are plotted in Fig. 2. The assumption that the ice particles are solid ice is known to be wrong, but the precise form of the ice density–size relationship is a matter of some debate and is discussed in the next section.

### 3. The effect of ice density on IWC inferred from $Z$

In the previous section we drew attention to the crucial role of the assumed density variation of the ice

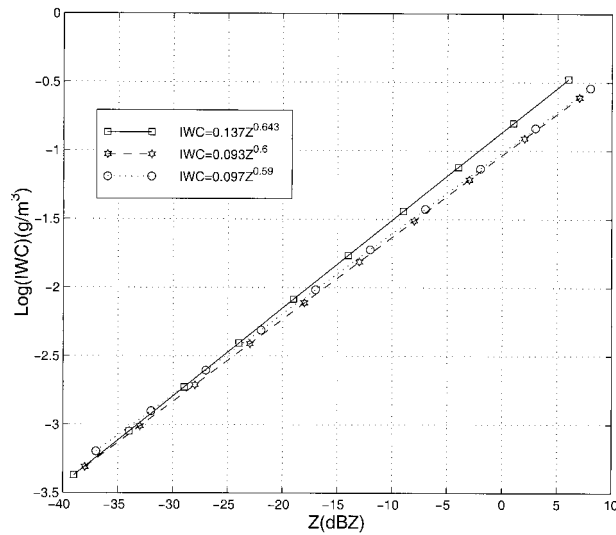


FIG. 2. Mean IWC– $Z$  relationships proposed for 94 GHz (solid line) and 35 GHz (dotted line) using the ice densities from Eq. (4). The dashed line is for 94 GHz and the densities from Eq. (9).

particles with their diameter when estimating  $Z$  and IWC. We now consider the role of density further, together with the effect of different methods of estimating the diameter of particles from the aircraft images. In addition, we need to consider the possible influence of particle shape. Ice particles and aggregates are known to be aspherical, but the larger particles that contribute most to the reflectivity have a lower density and therefore a reduced refractive index so they reflect microwaves as if they were spherical. We conclude that the precise shape of the ice particles may be neglected when calculating the radar reflectivity.

All the computations are carried out at 94 GHz and the Maxwell–Garnett (1904) formulas for calculating the refractive index of ice–air mixtures is used. We shall examine these sensitivities using the EUCREX and the CEPEX aircraft data that are described in detail by Brown et al. (1995). The EUCREX dataset comprises a total of 14 704 5-s averaged size spectra from a total of approximately 9200 km of flight, measured at temperatures between  $-10^{\circ}\text{C}$  and  $-50^{\circ}\text{C}$  associated with frontal ice cloud around the United Kingdom. The CEPEX dataset sampled tropical ice clouds. This dataset comprises 12 506 10-s averaged size spectra from approximately 24 000 km of horizontal flight measured at temperatures between  $-10^{\circ}\text{C}$  and  $-65^{\circ}\text{C}$ . In both the EUCREX and CEPEX campaigns, the weather condition, cloud temperature, particle size distribution, and other related parameters were measured. The ice crystal size spectra were measured using two 2D Optical Array Probes (Knollenberg 1970) for particle sizes from 25 to 800  $\mu\text{m}$  (2D-C) and from 200 to 6400  $\mu\text{m}$  (2D-P). This EUCREX dataset we use is slightly larger than the one used by Brown et al. (1995).

In the FIRE data, Atlas et al. (1995) categorized the

crystals using the longest dimension of the particle image recorded either perpendicular or parallel to the axis of the 2D probe. To account for the fact that they were somewhat irregular, this length was multiplied by 0.9 to give an estimate of  $D$  for the equivalent sphere. In CEPEX the  $D$  value was taken as the major axis of the image. To check the sensitivity to this change, the values of  $D$  in the CEPEX spectra were all multiplied by 0.9 and the values of  $Z$  and IWC were recomputed and fitted to a relationship of the form  $\text{IWC} = aZ^b$ . The original formula [Eq. (6a)] was  $\text{IWC} = 0.137Z^{0.643}$ , but reducing  $D$  by 0.9 increased  $a$  to 0.158, or by 10%.

It seems unlikely that the density of the larger particles, which may be growing by aggregation, should continue to decrease indefinitely as the size increases. As a first test of the sensitivity to the density of the larger particles, the density decrease in Eq. (4) was truncated at a minimum value of  $0.1 \text{ g cm}^{-3}$  and the  $Z$  and IWC values from the individual spectra recalculated. When the data were fitted, the value of  $b$  was unchanged but the coefficient  $a$  was reduced to 0.126. In other words, for a given  $Z$  the value of IWC was reduced by less than 10% for a minimum density of  $0.1 \text{ g cm}^{-3}$ . Truncating at  $0.05 \text{ g cm}^{-3}$  had a negligible effect on either coefficient.

The unknown density of the larger ice particles remains a major uncertainty in this analysis. Brown and Francis (1995) compared bulk IWC measurements from the Total Water Probe with those calculated from the 2D spectra and found equally good agreement for mass–diameter relationships  $m = 0.002938D^{1.9}$  for “aggregates of unrimed bullets, columns, and side planes” and  $m = 0.00769D^{2.27}$  for bullet–rosette crystals (Mitchell et al. 1990) where  $m$  is in grams and  $D$  is in centimeters. If  $D$  is taken as the diameter of the equivalent volume sphere, then these two relationships lead, respectively, to density–size formulas given by Eq. (4) and by

$$\rho = 0.078D^{-0.73}, \quad (7)$$

where  $D$  is in millimeters. They also tried a relationship of the form  $m = 0.0829D^{2.6}$ , which leads to the density–size formula

$$\rho = 0.396D^{-0.4}. \quad (8)$$

This density is definitely too high for the larger ice particles as the ice content computed from the 2D probes is over four times larger than that given by the total water probe. The density–size equations, 4, 7, and 8 are displayed in Fig. 3.

Francis et al. (1998) reanalyzed the data used by Brown and Francis but adopted a different empirical approach in which they assumed that the diameter of the mass-equivalent water droplet,  $D_{\text{eq}}$ , was related to the cross-sectional area detected by the probe,  $A$ , by the formulas  $D_{\text{eq}} = aA^b$ , where  $D_{\text{eq}}$  is in centimeters and  $A$  is in square centimeters. They found very good unbiased agreement between the 2D-probe water content and that from the total water probe, for values of  $a = 0.615$  and

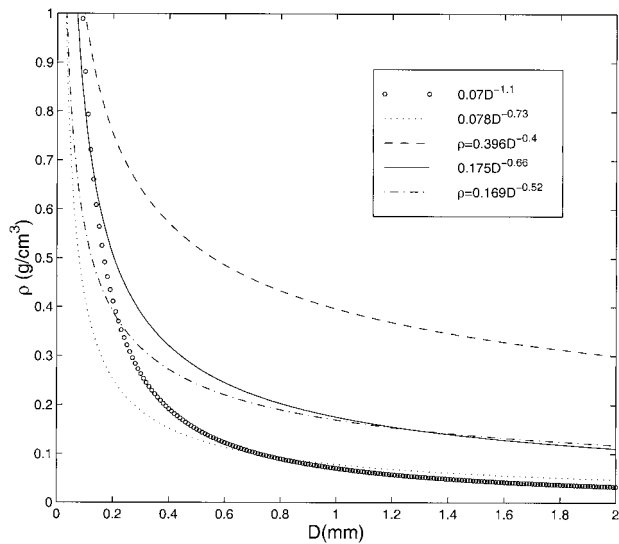


FIG. 3. The various ice densities vs size relationships discussed in the text. Solid line, Eq. (4). Dotted line, Eq. (7). Dashed lines, Eqs. (9) and (10). Dash-dot line, Eq. (8).

$b = 0.39$ . Hogan et al. (2000) assumed an actual particle diameter,  $D$ , given by  $A = \pi D^2/4$ , to calculate a particle volume, and derived a density-size formula

$$\rho = 0.175D^{-0.66}, \quad (9)$$

which is significantly different from (4) for crystals with diameters of 300  $\mu\text{m}$  and more. The difference arises because for a nonspherical particle the value of  $D$  calculated from the cross-sectional area is less than that from the mean of the two dimensions parallel and perpendicular to the probe array as used by Brown and Francis (1995).

Another widely used relationship due to Mitchell (1996) for “side planes” is  $m = 0.004 19D^{2.3}$ ; for these particles he reports that the measured particle area is related to the diameter (both in cm) by  $A = 0.2285D^{1.88}$ . If this diameter is used to calculate the volume, then we have a density variation

$$\rho = 0.169D^{-0.52}, \quad (10)$$

which, as shown in Fig. 3, is very similar to Eq. (9).

To check the sensitivity of  $Z$ -IWC relationship to the higher densities of Eq. (9) inferred by Francis et al. (1998), the values of  $Z$  and IWC for the individual CEPEX spectra were recalculated using the new densities. The higher densities for the larger particles lead to a relationship  $\text{IWC} = 0.093 Z^{0.6}$ , which is also plotted in Fig. 2. In other words for a  $Z$  of 0 dBZ, the value of IWC is about 30% lower using the density in Eq. (9) than it is for Eq. (4); at  $-20$  dBZ the change is only 20%. In this case truncating the density at a minimum value of  $0.1 \text{ g cm}^{-3}$  and  $0.05 \text{ g cm}^{-3}$  only affects the very largest ice particles and has no effect on the IWC- $Z$  relationship.

If we compare the curves in Fig. 3, then the much higher densities of Eq. (8) are definitely wrong because they lead to an overestimate of the IWC of a factor of 4 when compared to direct IWC estimates. However, the higher densities of Eqs. (9) and (10) give as good agreement with the direct total IWC as do the lower density Eqs. (4) and (7), but lead to different IWC- $Z$  relationships as displayed in Fig. 2. The differences are up to 30% for the higher values of IWC of  $0.1 \text{ g m}^{-3}$ . At the lowest values of IWC of  $<0.001 \text{ g m}^{-3}$  there will be a contribution to the IWC by crystals that are too small to be detected by the aircraft probes, which will lead to the relationships in Fig. 2 underestimating the IWC for a given  $Z$ . With these caveats in mind, we will use the Eqs. (6a,b) as the optimum formulae for deriving the mean values of IWC from reflectivity.

Thus far we have discussed mean relationships between IWC and  $Z$ . Both Brown et al. (1995) and Atlas et al. (1995) found that the individual estimates of IWC for the  $Z$  of a particular spectrum were log-normally distributed around the mean IWC- $Z$  curve and that the standard deviation of the individual  $\log(\text{IWC})$  estimate was about 0.3, or a factor of 2. The variation in the IWC- $Z$  relationship from day to day is well illustrated in Fig. 4. In 4a EUCREX data are plotted for flights A279, A189, and A193 demonstrating the large spread in IWC values for a given  $Z$ . Panel (4b) shows three regression lines representing fits for the three flights, together with the error bars defined as one standard deviation of the values of  $\log(\text{IWC})$  when the observations are split up into 2.5-dBZ intervals of reflectivity. The three lines differ from cloud to cloud (or day to day) as pointed out by Atlas et al. (1995).

#### 4. Classification by $D^*$ and temperature

Both Atlas et al. (1995) and Brown et al. (1995) noted that when ice particle spectra were sorted into different values of  $D^*$  then the spread of calculated IWC for a given  $Z$  was considerably reduced. Brown et al. found that the random error was typically reduced to +50% and -35%. However, the characteristic particle diameter  $D^*$  is an unknown parameter that has to be inferred, for example, from the radar/lidar backscatter ratio (Intrieri et al. 1993) or dual-wavelength radar measurements (Hogan et al. 2000). These techniques both have practical limitations. The lidar returns can be affected by attenuation and multiple scattering. Both techniques rely on the two beamwidths and sample volumes being matched. Instead we now investigate a much simpler technique: the use of temperature as a means of classifying the IWC- $Z$  relationships. Temperature has the advantage that it can be simply related to the altitude either from a forecast analysis, or in the Tropics, a climatological value may suffice. Heymsfield and Platt (1984) and Kosarev and Mazin (1991) reported that there was systematic dependence on particle size spectral form with temperature. Ou and Liou (1995) derived

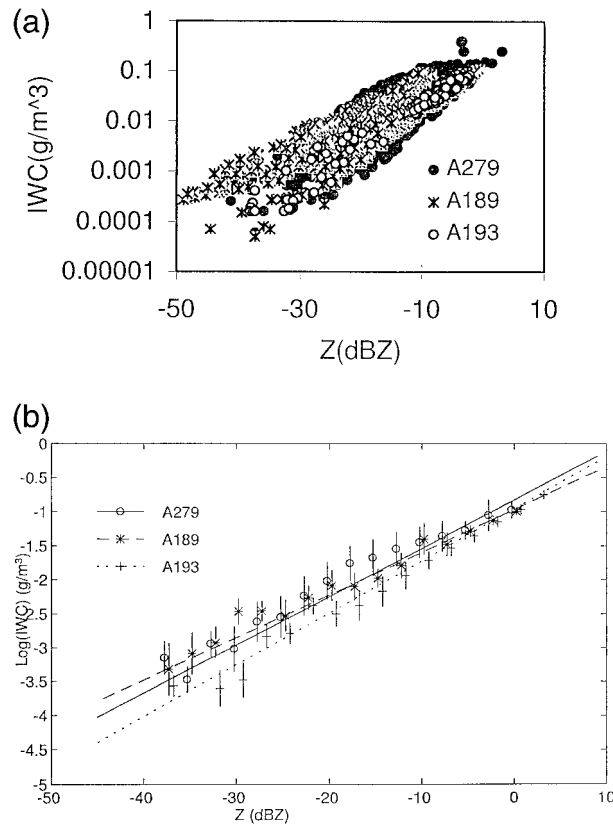


FIG. 4. IWC–Z relations for three EUCREX flights. (a) Scatterplot of IWC–Z values for individual spectra for three flights. (b) Three fits of IWC–Z for the three different flights. The mean and standard deviation of log(IWC) for each 2.5-dBZ interval in Z is displayed for each flight.

a relationship between crystal size and temperature based on Heymsfield and Platt (1984) data and it is interesting to note that this temperature-dependent size is used in the ice parameterization scheme of the current ECMWF operational model (D. Gregory 1998, personal communication). McFarquhar and Heymsfield (1997) analyzed the CEPEX dataset and found again a systematic variation of ice water content, and hence ice particle size spectra with temperature. The spread of the data was so large that they comment that IWC and size distributions cannot be parameterized as functions of *T* alone. We now consider the errors in deriving ice water content when the spectra are categorized in terms of both their temperature and their radar reflectivity.

To analyze the IWC–Z dependence on temperature, the values of IWC and Z from all the individual spectra recorded from EUCREX and CEPEX data using the density function from Eq. (4) were sorted into 6 K steps of temperature. The results together with the fitted lines are displayed in Figs. 5 and 6. A temperature step of 6 K corresponds to approximately 1 km change in altitude, so if the altitude of the radar reflectivity is known, then the temperature could be ascertained to this accuracy

from an operational numerical model. Both figures indicate that the highest density of data points shifts from bottom-left to top-right as the temperature increases, implying that the higher IWCs tend to occur at higher values of the temperature. As the temperature rises the fitted lines tend to move down toward the bottom-right corner of the plots consistent with an increase in mean particle size. The effect is small but significant; for a Z of –30 dBZ the value of IWC at the highest temperature is appreciably lower than that for the temperature 48 K lower.

An alternative representation of the derived values of IWC from Z when the data are classified by temperature is given in Figs. 7 and 8 for the EUCREX and CEPEX data, respectively. In these figures the data have been split into 2.5 dB steps in Z and the mean value of log(IWC) and its standard deviation derived for each of nine 6 K steps in temperature spanning the range 216–270 K. For clarity, the three curves in each panel are for three temperature steps each separated by 18 K, and from one panel to the next the temperatures of the three curves are increased by 6 K. The figures confirm that classification in terms of temperature leads to distinctly different Z–IWC relationships at different temperatures and show a significant reduction in errors of derived IWC if the data are classified by temperature and reflectivity, so this may be a useful tool for providing more accurate estimates of IWC. Note that although IWC and Z both generally increase with temperature, Figs. 7 and 8 show that, for a given Z, the value of IWC is larger at the lower temperatures reflecting the generally smaller ice particles at lower temperatures.

Tables 2 and 3 provide quantitative magnitudes for the mean value of log(IWC) and its standard deviation for the EUCREX and CEPEX datasets as plotted in Figs. 7 and 8. The errors are quoted only for those entries in the table based on more than 4 data points: the unbracketed entries for more than 20 points can be considered the most reliable. A standard deviation of 0.1 corresponds to a +25%/–20% error and a deviation of 0.2 to an error of about +58%/–37%. Note that some of the error will be contributed by the finite spread of 2.5 dB in the range of Z included in each classification; this would lead to 68% of the data points having an error in log(IWC) of more than 0.08 even if the real correlation between IWC and Z was perfect. Tables 2 and 3 also give values of log(IWC) and associated error for all the data within a given Z category for Mie scattering at 94 GHz and for Rayleigh scattering. For Rayleigh scattering the errors in log(IWC) are 0.3, or a factor of 2, for high values of Z, but rise to 0.4 or even 0.5 (factors of 2.5 and 3) for the lower values of Z. However, allowance for Mie scattering at 94 GHz leads to an increased value of IWC for a given Z and a reduction for errors particularly for the higher values of Z where the particles are likely to be larger (see Fig. 1a).

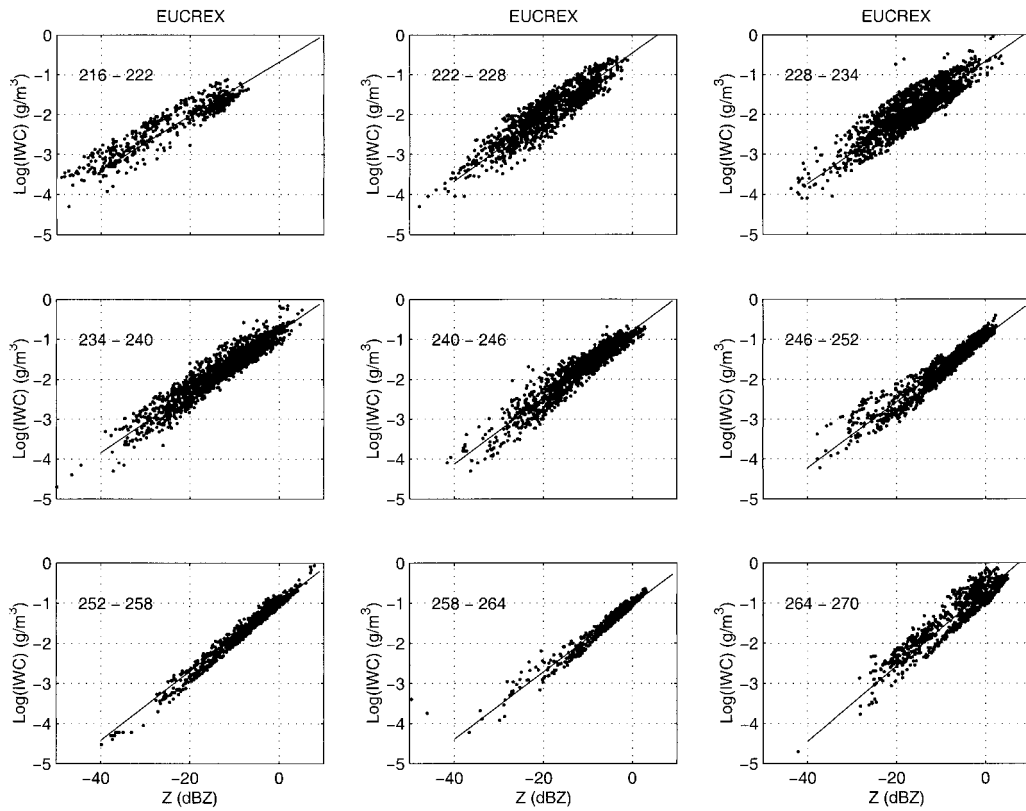


FIG. 5. Scatterplot of IWC-Z for EUCREX spectra with nine different temperature ranges.

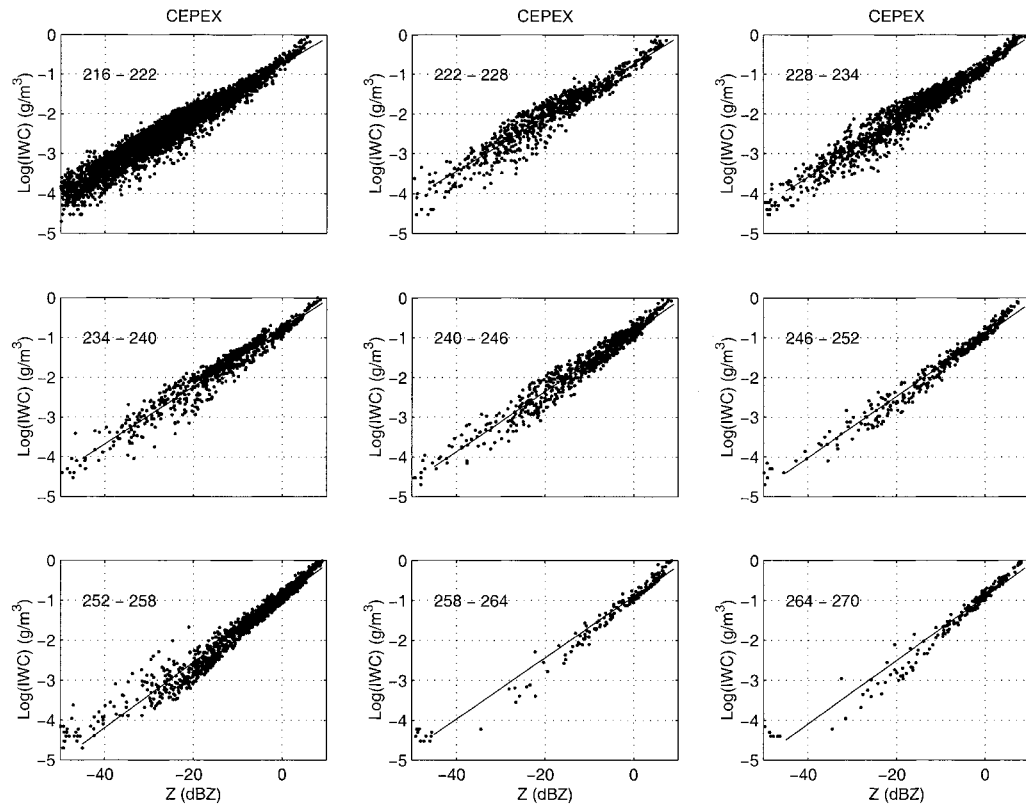


FIG. 6. As Fig. 5, but for CEPEX data.

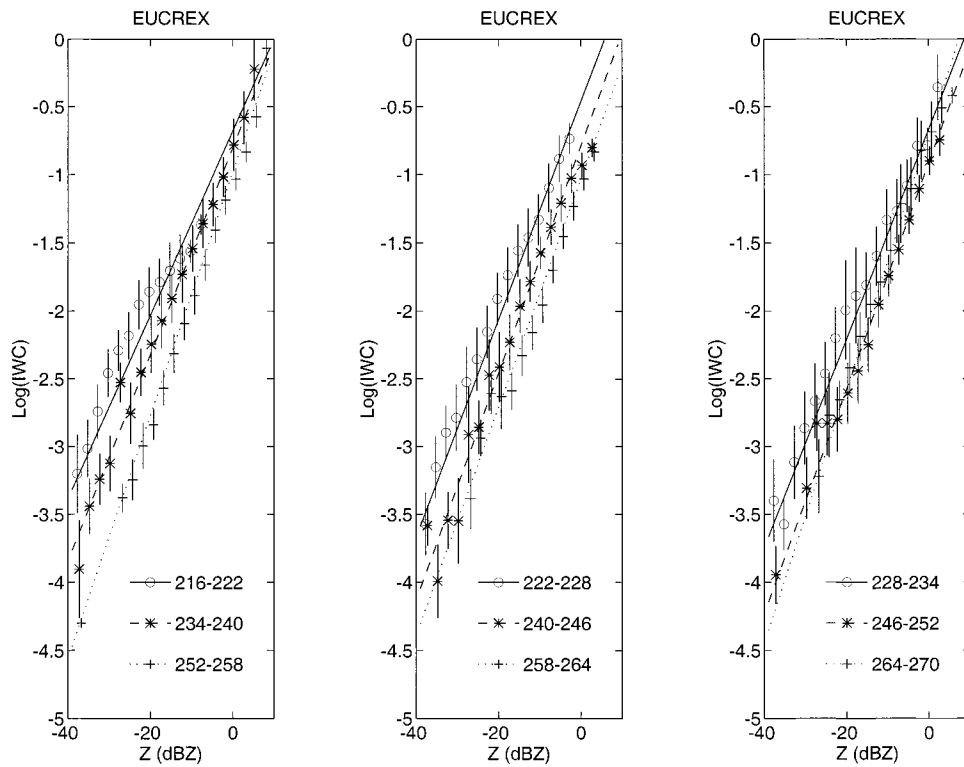


FIG. 7. Fitted IWC–Z lines for EUCREX data with the nine temperature ranges of Fig. 5, together with the mean log(IWC) values and the standard deviation for each 2.5-dB step in Z. For clarity, each panel has three curves for temperature ranges separated by 18 K; from one panel to the next the temperatures for the three curves increase by 6 K.

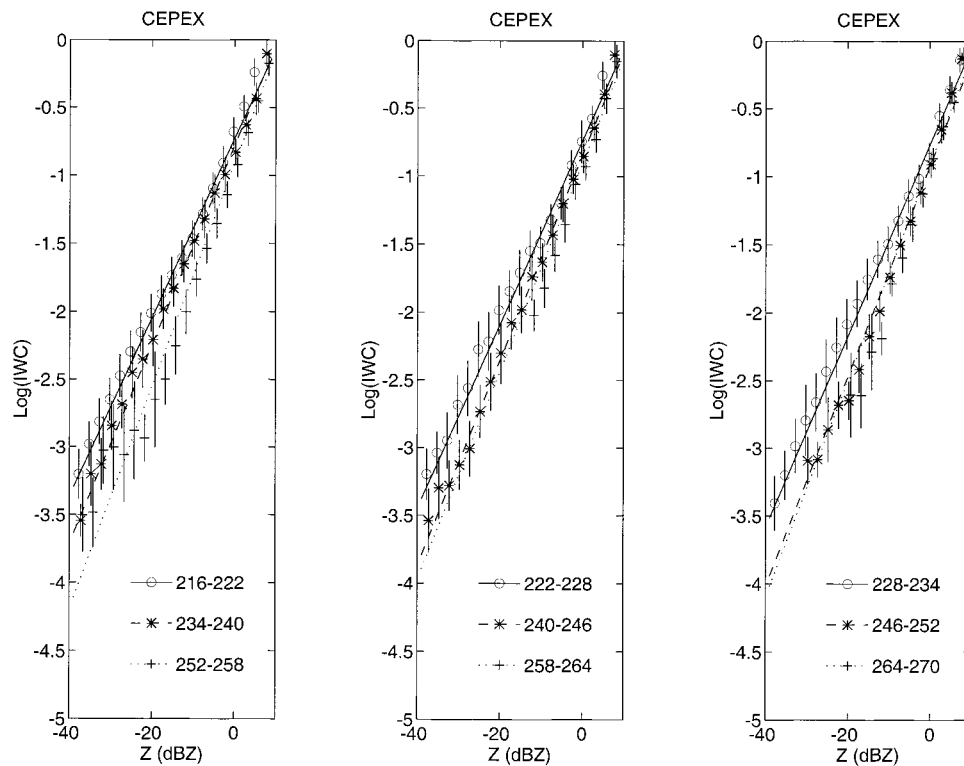


FIG. 8. As Fig. 7, but for CEPEX data.

TABLE 2. Mean value of log(IWC) and its standard deviation (EUCREX). Data point ranges: (10 > n ≥ 5), [20 > n ≥ 10], open n ≥ 20.

<i>T</i> (K) (±3) <i>Z</i> (dBZ) (±1.25)	219	225	231	237	243
9.75					
7.25					
4.75				(−0.29 ± 0.27)	
2.25			(−0.46 ± 0.32)	[−0.63 ± 0.20]	−0.81 ± 0.07
−0.25			(−0.81 ± 0.16)	−0.82 ± 0.18	−0.94 ± 0.10
−2.75		[−0.77 ± 0.15]	−0.87 ± 0.27	−1.05 ± 0.16	−1.04 ± 0.12
−5.25		−0.94 ± 0.24	−1.15 ± 0.24	−1.25 ± 0.15	−1.24 ± 0.16
−7.75	(−1.37 ± 0.08)	−1.15 ± 0.21	−1.35 ± 0.26	−1.40 ± 0.18	−1.41 ± 0.15
−10.25	−1.57 ± 0.98	−1.38 ± 0.20	−1.42 ± 0.27	−1.58 ± 0.18	−1.60 ± 0.15
−12.75	−1.65 ± 0.17	−1.53 ± 0.25	−1.68 ± 0.26	−1.78 ± 0.19	−1.82 ± 0.19
−15.25	−1.76 ± 0.20	−1.62 ± 0.25	−1.89 ± 0.24	−1.95 ± 0.19	−2.04 ± 0.26
−17.75	−1.83 ± 0.19	−1.83 ± 0.31	−2.01 ± 0.29	−2.13 ± 0.21	−2.30 ± 0.24
−20.25	−1.92 ± 0.26	−1.99 ± 0.29	−2.11 ± 0.29	−2.32 ± 0.25	−2.53 ± 0.32
−22.75	−2.02 ± 0.27	−2.23 ± 0.26	−2.31 ± 0.33	−2.51 ± 0.25	−2.60 ± 0.35
−25.25	−2.26 ± 0.29	−2.47 ± 0.33	−2.57 ± 0.31	−2.84 ± 0.28	−2.93 ± 0.26
−27.75	−2.34 ± 0.24	−2.66 ± 0.35	−2.79 ± 0.31	−2.59 ± 0.28	−3.07 ± 0.33
−30.25	−2.53 ± 0.29	−2.90 ± 0.33	−3.00 ± 0.33	−3.19 ± 0.23	−3.64 ± 0.22
−32.75	−2.82 ± 0.28	−2.97 ± 0.28	−3.22 ± 0.28	−3.30 ± 0.22	−3.60 ± 0.22
−35.25	−3.10 ± 0.26	−3.29 ± 0.24	−3.63 ± 0.23	−3.50 ± 0.23	−4.03 ± 0.14
−37.75	−3.41 ± 0.45	−3.68 ± 0.33	[−3.55 ± 0.34]	−4.12 ± 0.37	−3.62 ± 0.17

Brown et al. (1995) reported a reduction in the error of log(IWC) were categorized in terms of *D\** and Tables 2 and 3 reveal that temperature classification leads to comparable error reduction. For example, if *Z* is around −3 dBZ, then *D\** classification reduces the error from 0.18 to about 0.15 and 0.1 for EUCREX and CEPEX, respectively, and the *T* classification yields a figure of around 0.12. If *Z* is −15 dBZ, then sorting in terms of *D\** reduces the original error of around 0.3 to values between 0.15 and 0.2, whereas sorting in terms of *T* leads to errors in the range around 0.2. For a *Z* of around

−28 dBZ the *D\** classification reduces an original error of 0.4 in the EUCREX data to around 0.2 and *T* reduces it to around 0.3; for CEPEX data the spread of recorded temperatures at this value of *Z* is insufficient for this analysis. These data are also displayed in Figs. 9 and 10. In both figures the symbols representing the standard deviation for different temperature ranges (i.e., the data in Table 2 and 3), where the standard deviations in log(IWC) are derived from data subdivided for each 2.5 dBZ step in *Z* and each 6 K temperature step. Figure 9 is for EUCREX data with the separate panels displaying

TABLE 3. Mean value of log (IWC) and its standard deviation (CEPEX). Data point ranges: (10 > n ≥ 5), [20 > n ≥ 10], open n ≥ 20.

<i>T</i> (K) (±3) <i>Z</i> (dBZ) (±1.25)	219	225	231	237	243
9.75				[0.08 ± 0.06]	
7.25			−0.15 ± 0.10	[−0.11 ± 0.10]	[−0.12 ± 0.11]
4.75	[−0.25 ± 0.11]	−0.29 ± 0.14	−0.37 ± 0.11	−0.45 ± 0.12	−0.41 ± 0.11
2.25	−0.50 ± 0.09	−0.59 ± 0.11	−0.56 ± 0.10	−0.64 ± 0.09	−0.66 ± 0.11
−0.25	−0.70 ± 0.12	[−0.78 ± 0.16]	−0.88 ± 0.11	−0.84 ± 0.11	−0.88 ± 0.13
−2.75	−0.93 ± 0.15	−0.94 ± 0.13	−1.03 ± 0.12	−1.02 ± 0.16	−1.04 ± 0.13
−5.25	−1.11 ± 0.13	−1.22 ± 0.14	−1.17 ± 0.16	−1.16 ± 0.16	−1.23 ± 0.16
−7.75	−1.31 ± 0.15	−1.34 ± 0.13	−1.35 ± 0.14	−1.36 ± 0.18	−1.46 ± 0.16
−10.25	−1.49 ± 0.16	−1.51 ± 0.13	−1.52 ± 0.15	−1.52 ± 0.18	−1.66 ± 0.15
−12.75	−1.63 ± 0.16	−1.58 ± 0.18	−1.64 ± 0.18	−1.68 ± 0.16	−1.79 ± 0.23
−15.25	−1.77 ± 0.18	−1.75 ± 0.21	−1.79 ± 0.18	−1.87 ± 0.21	−2.02 ± 0.20
−17.75	−1.90 ± 0.18	−1.89 ± 0.21	−1.99 ± 0.24	−2.04 ± 0.23	−2.15 ± 0.27
−20.25	−2.05 ± 0.18	−2.05 ± 0.27	−2.15 ± 0.26	−2.31 ± 0.34	−2.43 ± 0.34
−22.75	−2.20 ± 0.21	−2.31 ± 0.32	−2.35 ± 0.30	−2.44 ± 0.30	−2.60 ± 0.29
−25.25	−2.35 ± 0.23	−2.38 ± 0.35	−2.55 ± 0.35	−2.54 ± 0.33	−2.80 ± 0.26
−27.75	−2.53 ± 0.23	−2.64 ± 0.29	−2.73 ± 0.26	−2.76 ± 0.30	[−3.08 ± 0.26]
−30.25	−2.70 ± 0.22	−2.77 ± 0.29	−2.90 ± 0.31	[−2.91 ± 0.26]	(−3.20 ± 0.28)
−32.75	−2.87 ± 0.24	−3.05 ± 0.34	−3.05 ± 0.25	[−3.22 ± 0.32]	(−3.35 ± 0.27)
−35.25	−3.03 ± 0.23	[−3.08 ± 0.21]	−3.26 ± 0.24	[−3.29 ± 0.30]	(−3.37 ± 0.26)
−37.75	−3.27 ± 0.24	[−3.27 ± 0.27]	−3.48 ± 0.26	(−3.57 ± 0.15)	(−3.64 ± 0.33)

TABLE 2. (Extended)

249	255	261	267	Mie	Rayleigh
					-0.94 ± 0.21
	(-0.08 ± 0.14)			-0.08 ± 0.14	-1.04 ± 0.26
	[-0.58 ± 0.09]			-0.44 ± 0.11	-1.15 ± 0.20
-0.76 ± 0.11	-0.84 ± 0.08	-0.84 ± 0.07	-0.43 ± 0.06	-0.68 ± 0.19	-1.28 ± 0.21
-0.91 ± 0.11	-1.04 ± 0.09	-1.04 ± 0.09	-0.76 ± 0.24	-0.93 ± 0.18	-1.41 ± 0.26
-1.12 ± 0.11	-1.20 ± 0.11	-1.25 ± 0.11	-0.91 ± 0.27	-1.09 ± 0.19	-1.49 ± 0.30
-1.35 ± 0.12	-1.42 ± 0.10	-1.47 ± 0.10	-1.20 ± 0.29	-1.30 ± 0.19	-1.55 ± 0.37
-1.57 ± 0.13	-1.68 ± 0.12	-1.71 ± 0.11	-1.38 ± 0.36	-1.44 ± 0.23	-1.57 ± 0.38
-1.78 ± 0.18	-1.91 ± 0.15	-1.98 ± 0.16	-1.68 ± 0.30	-1.58 ± 0.25	-1.68 ± 0.36
-2.00 ± 0.20	-2.11 ± 0.14	-2.18 ± 0.14	-1.87 ± 0.28	-1.77 ± 0.27	-1.86 ± 0.36
-2.31 ± 0.23	-2.34 ± 0.16	[-2.36 ± 0.16]	-2.00 ± 0.21	-1.94 ± 0.29	-2.02 ± 0.39
-2.53 ± 0.25	-2.59 ± 0.14	[-2.61 ± 0.15]	-2.25 ± 0.24	-2.11 ± 0.34	-2.15 ± 0.48
-2.69 ± 0.25	-2.86 ± 0.13	[-2.72 ± 0.29]	-2.50 ± 0.29	-2.24 ± 0.38	-2.23 ± 0.46
-2.88 ± 0.25	-3.04 ± 0.20	(-2.65 ± 0.20)	-2.69 ± 0.18	-2.44 ± 0.37	-2.57 ± 0.62
-2.92 ± 0.28	[-3.27 ± 0.14]	(-2.96 ± 0.15)	-3.02 ± 0.47	-2.71 ± 0.40	-2.69 ± 0.48
-2.93 ± 0.32	[-3.40 ± 0.13]	-3.48 ± 0.30	[-3.36 ± 0.35]	-2.76 ± 0.41	-2.71 ± 0.53
-3.40 ± 0.27				-3.20 ± 0.52	-2.96 ± 0.54
				-3.21 ± 0.38	-3.24 ± 0.55
				-3.60 ± 0.42	-3.75 ± 0.57
-3.98 ± 0.15	-4.30 ± 0.02			-3.78 ± 0.46	-3.77 ± 0.63

the same classification by temperature, but for different values of  $D^*$  with various line styles representing different widths of the class of  $D^*$  data deemed acceptable. In this figure the width of the class varies from 10 to 70  $\mu\text{m}$  around the central value. For example, the dotted line in the top left-hand side of the figure represents a standard deviation of  $\log(\text{IWC})$  for all data with a  $D^*$  of  $35 \pm 5 \mu\text{m}$ . Figures 9 confirms that the errors for using  $D^*$  and  $T$  are broadly comparable, with the classification by  $D^*$  slightly outperforming the  $T$  technique at low  $Z$ . Increasing the spread of acceptable  $D^*$  only increases the standard error in the retrieved IWC by a

very small amount, confirming that the limit to the  $D^*$  accuracy is caused by deviations of real spectra from exponentiality. The CEPEX data are displayed in Figs. 10 and confirm that the  $D^*$  technique is marginally better than  $T$  for values of  $Z$  below  $-20 \text{ dBZ}$ , but for larger  $Z$  both techniques are comparable.

If we return to the Rayleigh scattering errors in Tables 2 and 3 then we find these are also reduced by  $T$  classification. The errors for EUCREX Rayleigh scattering in the table increase from about 0.25 at higher  $Z$  to close to 0.5 for  $Z$  of  $-30 \text{ dBZ}$ . Classification by  $T$  (not shown in the table) reduces these to about 0.15 and 0.3, re-

TABLE 3. (Extended)

249	255	261	267	Mie	Rayleigh
	0.10 ± 0.10	(0.05 ± 0.04)	(0.03 ± 0.01)	0.08 ± 0.08	-0.53 ± 0.28
(-0.13 ± 0.05)	-0.18 ± 0.10	[-0.17 ± 0.14]	(-0.12 ± 0.08)	-0.16 ± 0.10	-0.69 ± 0.29
-0.39 ± 0.09	-0.47 ± 0.10	-0.44 ± 0.11	[-0.46 ± 0.08]	-0.41 ± 0.12	-0.85 ± 0.30
-0.67 ± 0.11	-0.70 ± 0.10	[-0.74 ± 0.10]	-0.64 ± 0.10	-0.65 ± 0.12	-0.98 ± 0.28
-0.92 ± 0.10	-0.93 ± 0.10	-0.94 ± 0.11	-0.87 ± 0.09	-0.88 ± 0.13	-1.12 ± 0.34
-1.13 ± 0.10	-1.16 ± 0.11	[-1.07 ± 0.12]	-1.14 ± 0.10	-1.06 ± 0.16	-1.24 ± 0.32
-1.34 ± 0.12	-1.37 ± 0.12	[-1.38 ± 0.15]	[-1.37 ± 0.14]	-1.24 ± 0.18	-1.37 ± 0.29
-1.52 ± 0.11	-1.56 ± 0.13	[-1.60 ± 0.13]	[-1.61 ± 0.12]	-1.42 ± 0.18	-1.51 ± 0.31
-1.76 ± 0.14	-1.79 ± 0.16	[-1.85 ± 0.16]	[-1.80 ± 0.10]	-1.58 ± 0.20	-1.67 ± 0.36
-2.02 ± 0.18	-2.05 ± 0.18	(-2.04 ± 0.12)	(-2.21 ± 0.14)	-1.73 ± 0.25	-1.79 ± 0.37
[-2.21 ± 0.19]	-2.32 ± 0.23		(-2.41 ± 0.33)	-1.91 ± 0.30	-1.91 ± 0.39
[-2.46 ± 0.20]	-2.55 ± 0.21		(-2.68 ± 0.25)	-2.05 ± 0.32	-2.02 ± 0.40
(-2.68 ± 0.15)	-2.77 ± 0.29	-2.66 ± 0.16		-2.20 ± 0.35	-2.14 ± 0.42
[-2.74 ± 0.25]	-2.98 ± 0.21	-2.93 ± 0.58		-2.33 ± 0.34	-2.22 ± 0.40
[-2.96 ± 0.28]	-3.04 ± 0.33	-3.28 ± 0.17		-2.46 ± 0.35	-2.33 ± 0.41
(-3.11 ± 0.15)	-3.24 ± 0.37	-3.32 ± 0.20		-2.62 ± 0.33	-2.47 ± 0.38
(-3.14 ± 0.24)	[-3.17 ± 0.37]			-2.77 ± 0.30	-2.60 ± 0.35
	(-3.19 ± 0.48)			-2.91 ± 0.29	-2.72 ± 0.36
	(-3.59 ± 0.31)	-4.22 ± 0.00		-3.07 ± 0.29	-2.85 ± 0.33
	(-3.61 ± 0.32)			-3.26 ± 0.28	-3.03 ± 0.33

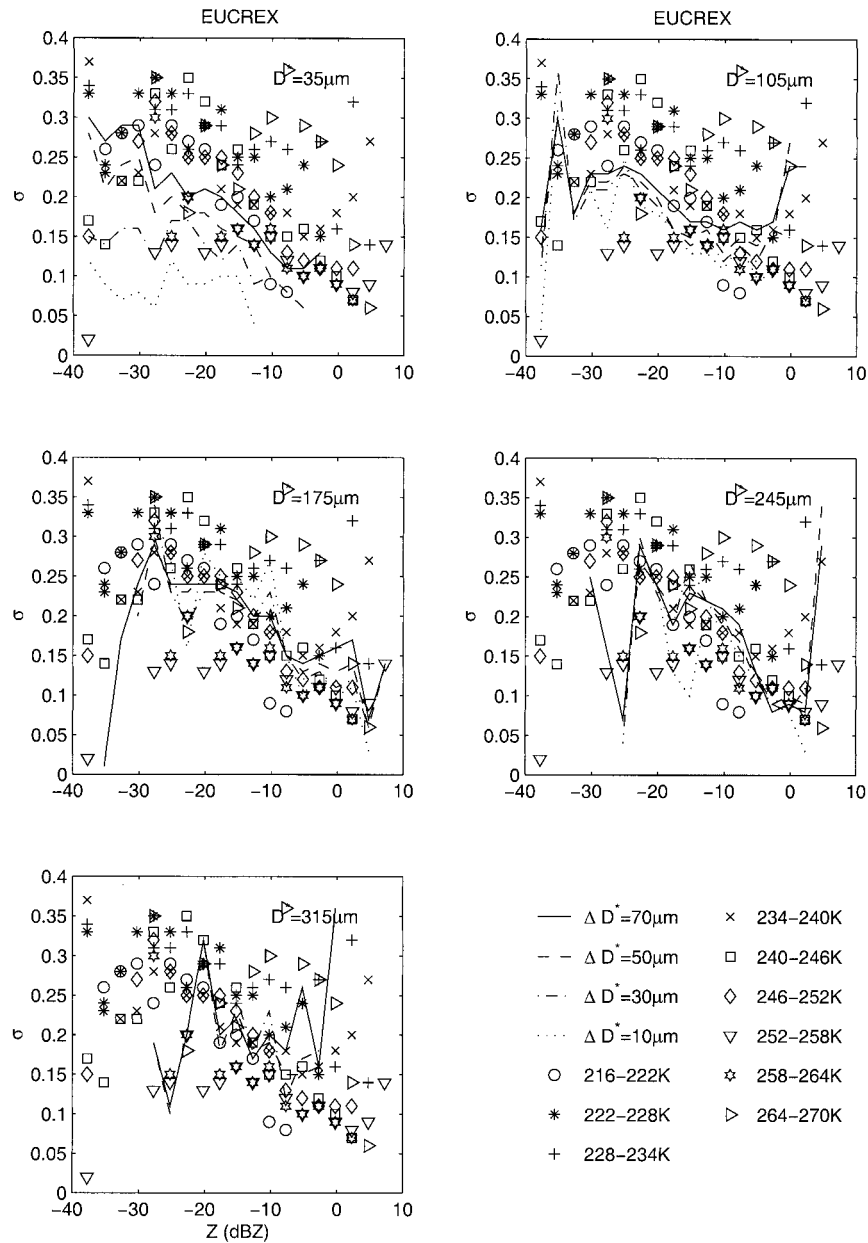


FIG. 9. Standard deviation of  $\log(\text{IWC})$  calculated from  $Z-D^*$  and  $Z-T$  for EUCREX data for each 2.5-dB step in  $Z$ . The symbols are for  $T$  classification, and lines are for  $D^*$  classification.  $\Delta D^*$  is the range of acceptable values of  $D^*$ .

spectively. The original CEPEX errors in Table 3 range from 0.3 for  $Z$  near 0 dBZ to 0.4 for a  $Z$  of  $-20$  dBZ; for  $Z$  below this value the errors are less, but this reflects the small range of temperatures sampled for low  $Z$  in this dataset. Classification by temperature reduces these errors in  $\log(\text{IWC})$  of 0.3 and 0.4 to about 0.2 and 0.3, respectively.

Table 4 displays the difference in the mean values of  $\log(\text{IWC})$  for a given  $Z$  and  $T$  for the midlatitude and equatorial datasets. The errors in parenthesis are for those

entries consisting of between 5 and 10 data points, and the errors in square brackets are for between 10 and 20 data points. The other entries are derived from more than 20 data points. If we consider those entries that correspond to more than 20 recorded data points, then nearly all the differences in the mean of  $\log(\text{IWC})$  are below 0.1 (i.e.,  $+25\%/-20\%$ ) and often they are below 0.05 ( $+12\%/-10\%$ ), indicating a small geographical bias. In general, the geographical bias is less than 25%. The values of the coefficients in the expression  $\text{IWC} = aZ^b$  for

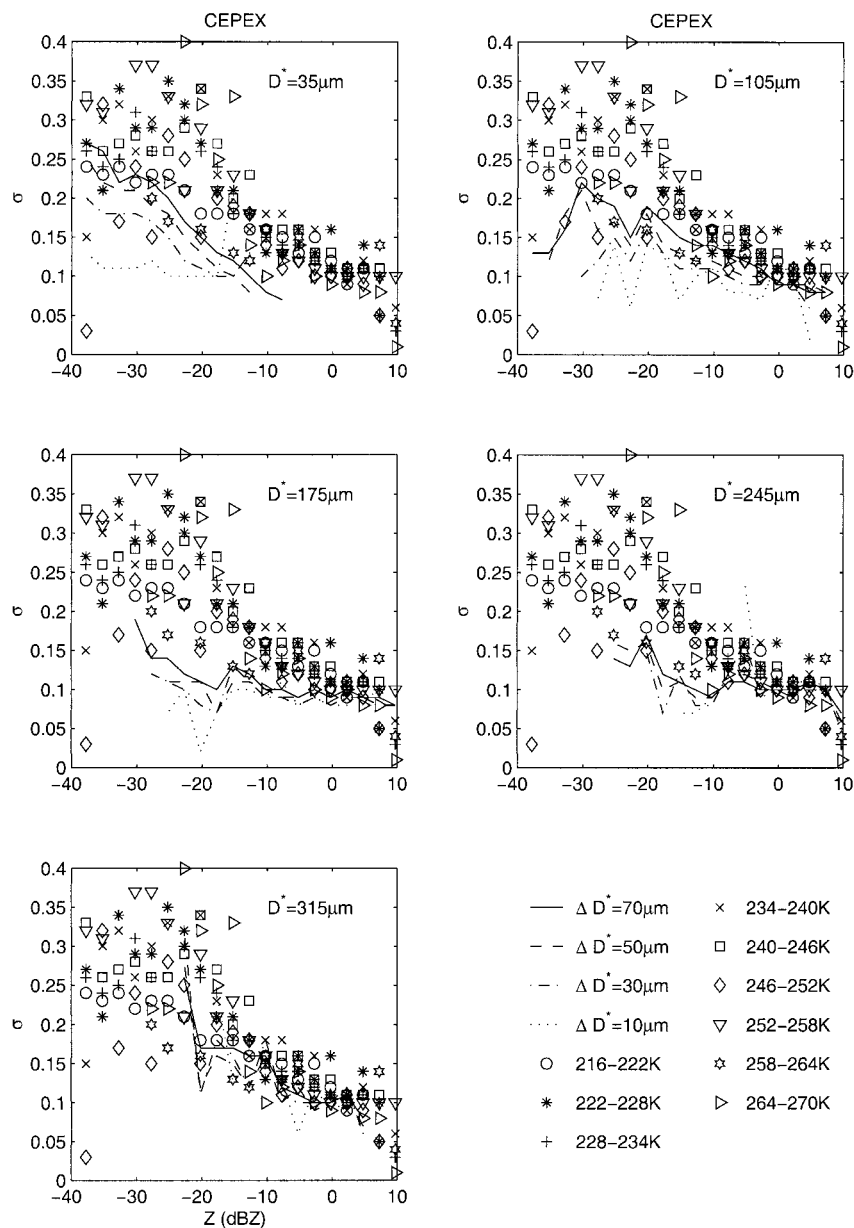


FIG. 10. As for Fig. 9 but for CEPEX data.

when  $Z$  is classified in terms of  $D^*$  and  $T$  are given in Table 5. The  $Z-D^*$  values are not significantly different from those of Brown et al. (1995), but because of the inability of the 2D probes to detect the smallest crystals the lowest values of  $D^*$  may be somewhat in error.

In order to establish the optimum temperature accuracy needed, the calculations of  $Z$  and IWC for the various spectra have been repeated in which the temperature band was set to 3, 6, and 12 K. As an initial check the mean  $\log(\text{IWC})$  values were calculated as a function of  $Z$  for the EUCREX and CEPEX datasets for the three different temperature steps. The values were nearly

identical, so different temperature steps have negligible effect on the mean IWC derivation. The corresponding errors of  $\log(\text{IWC})$  are plotted in Figs. 11 and 12. For EUCREX data in Fig. 11, there is a slight tendency for the error to increase for the largest temperature step, but for the CEPEX data there is no obvious reduction in error even when the 3 K step is used. Accordingly, a 6 K error in temperature (equivalent to about 1 km in height) is sufficient and there is nothing to be gained by using temperatures accurate to 3 K. Indeed if temperatures accurate to 12 K were all that was available then the degradation would not be severe.

TABLE 4. Mean log (IWC) value difference (EUCREX – CEPEX). Data point ranges: (10 > n ≥ 5), [20 > n ≥ 10], open n ≥ 20.

T (K) (±3) Z (dBZ) (±1.25)	219	225	231	237	243	249	225	261	267
9.75									
7.25									
4.75				(0.16)			[-0.11]		[0.03]
2.25			(0.10)	[0.01]	-0.15	-0.09	-0.14	[-0.10]	0.11
-0.25			(0.07)	0.02	-0.06	0.01	-0.11	-0.10	0.11
-2.75		[0.17]	0.16	[-0.03]	0.00	0.01	-0.04	[-0.18]	0.23
-5.25		0.28	0.02	-0.09	-0.01	-0.01	-0.05	[-0.09]	[0.17]
-7.75	(-0.06)	0.19	0.00	-0.04	0.05	-0.05	-0.12	[-0.11]	[0.23]
-10.25	-0.08	0.13	0.10	-0.06	0.06	-0.02	-0.12	[-0.13]	[0.12]
-12.75	-0.02	0.05	-0.04	-0.10	-0.03	0.02	-0.06	(-0.14)	(0.34)
-15.25	0.01	0.13	-0.10	-0.08	-0.02	[-0.10]	-0.02	[0.06]	(0.41)
-17.75	0.07	0.06	-0.02	-0.09	-0.15	[-0.07]	-0.04		(0.43)
-20.25	0.13	0.06	0.04	-0.01	-0.10	(-0.01)	-0.09		
-22.75	0.18	0.08	0.04	-0.07	0.00	[-0.14]	-0.06		
-25.25	0.09	-0.09	-0.02	(-0.30)	-0.13	[0.04]	[-0.23]		
-27.75	0.19	-0.02	-0.06	[0.17]	[0.01]	(0.18)	[-0.16]		
-30.25	0.17	-0.13	-0.10	(-0.28)	(-0.44)				
-32.75	0.05	0.08	-0.17	(-0.08)					
-35.25	-0.07	[-0.21]	-0.37	(-0.21)					
-37.75	-0.14	[-0.41]	[-0.07]						

5. Effect of spatial integration on retrieved IWC

Proposed radars for monitoring clouds from space operating at 94 GHz would have a footprint about 1 km in diameter but need to integrate in time to achieve sufficient sensitivity. Because of the movement of the satellite this integration time translates into a horizontal distance. Horizontal integration distances of 10 km have been proposed. Due to the inhomogeneous structure of ice clouds, and the nonlinear transformation from Z to IWC, it is expected that if Z is fluctuating then this average Z integrated over a distance will introduce some bias to the estimate of IWC.

TABLE 5. Constants a and b within different T and D\* ranges.

T(K)		EUCREX		CEPEX	
		a	b	a	b
216–222		0.2093	0.677	0.1854	0.658
222–228		0.3451	0.802	0.1827	0.677
228–234		0.2136	0.768	0.1716	0.705
234–240		0.1574	0.76	0.1648	0.723
240–246		0.1619	0.835	0.1440	0.757
246–252		0.1204	0.827	0.1192	0.774
252–258		0.1044	0.895	0.1215	0.819
258–264		0.09247	0.839	0.1254	0.767
264–270		0.2001	0.937	0.1235	0.797
D*(μm)	0–25	1.2699	0.8326	0.7723	0.7621
	25–50	1.2327	0.9460	0.7147	0.8498
	50–75	0.5374	0.9271	0.4449	0.8892
	75–100	0.2952	0.8935	0.3026	0.9019
	100–150	0.2223	0.9399	0.2100	0.9423
	150–200	0.1397	0.9209	0.1443	0.9530
	200–250	0.0990	0.8660	0.1179	0.9053
	250–300	0.1063	0.8730	0.1200	0.9715
	300–400	0.1084	0.7944	0.1121	0.9270
	400–500	0.1204	0.7906	0.0925	0.7917
	>500	0.2105	0.9382	0.1107	0.9369

In order to investigate the effect of integrating the radar reflectivity over a distance on the estimates of IWC, 14 704 EUCREX spectra for a total of around 100 level penetrations through ice clouds have been analyzed. An example of the data analysis from run number 1 of EUCREX flight A279 is shown in Fig. 13. Panel (a) is the linear average of radar reflectivity Z for integration distances of 1.25, 3.125, 5.0, 6.875, 8.75, and 10.62 km. The particle spectra were recorded every 5 s, and the aircraft speed was around 125 m s<sup>-1</sup>, so the corresponding number of integrated spectra is around 2, 5, 8, 11, 14, and 17, respectively. The plot in (b) is of the corresponding standard deviation of the average reflectivity when compared to the reflectivity of the individual unaveraged spectra. As expected the standard deviation of Z increases with integration distance.

The average of the value of log(IWC) calculated on the basis of the observed particle spectra is plotted in (c) for various integration distances. (d) is the error in log(IWC) from the averaged spectra when compared to the log(IWC) from the individual spectra. Finally, plotted in (e) is the fractional error in log(IWC) estimated via the averaged Z and the application of a Z–T equation using the coefficients in Table 5 when compared with the log(IWC) from the individual spectra over that distance. The fractional error in Fig. 13e represents the bias of the estimated IWC relative to the observed data. The error of log(IWC) for this penetration on flight A279 varies between about ±0.1 (or ±25%), but, for this penetration, the mean bias is about -0.03 (or about -7%) for all integration lengths.

A similar analysis has been carried out for all 104 EUCREX runs, and the frequency of the fractional error in derived log(IWC) calculated for the six different integration distances and for both Z–D\* and Z–T classi-

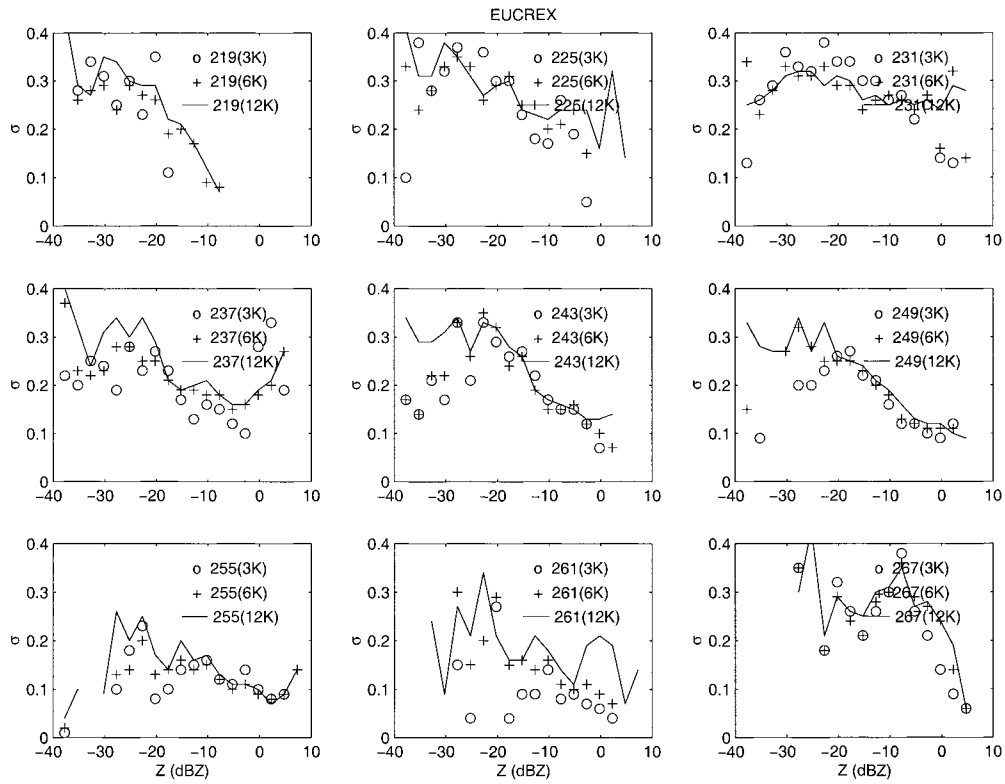


FIG. 11. The standard deviation of the estimate in  $\log(IWC)$  from Z and T for EUCREX data for different ranges of acceptable temperature:  $\Delta T = 3$  K (circles);  $\Delta T = 6$  K (plus signs);  $\Delta T = 12$  K (solid line).

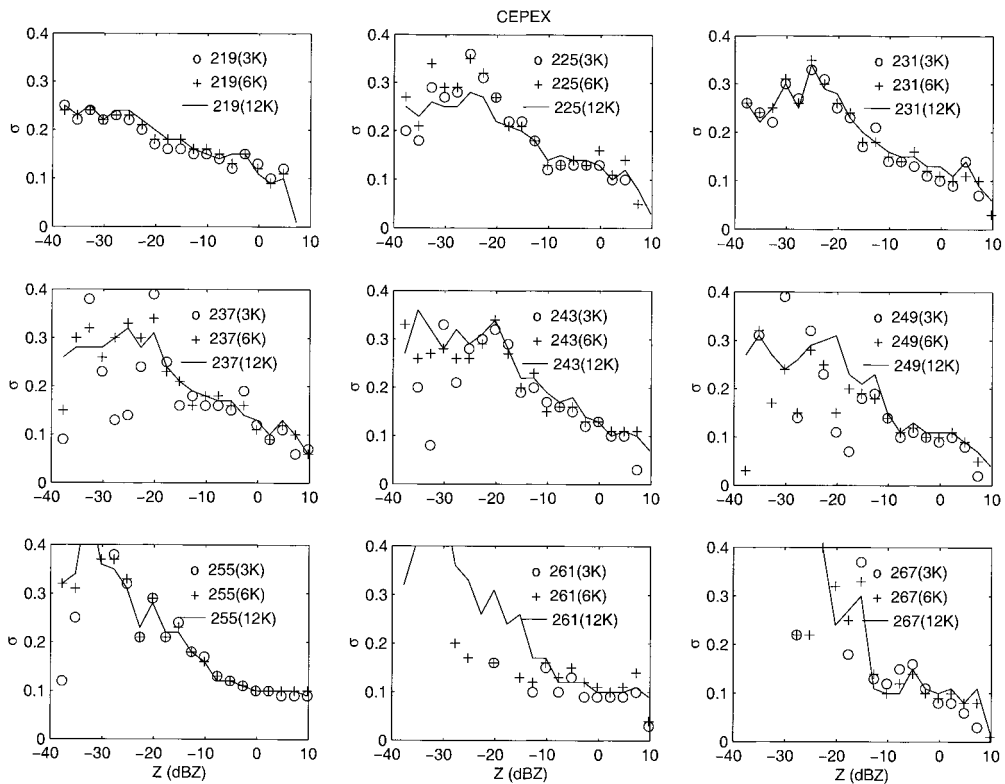


FIG. 12. As Fig. 11, but for CEPEX data.

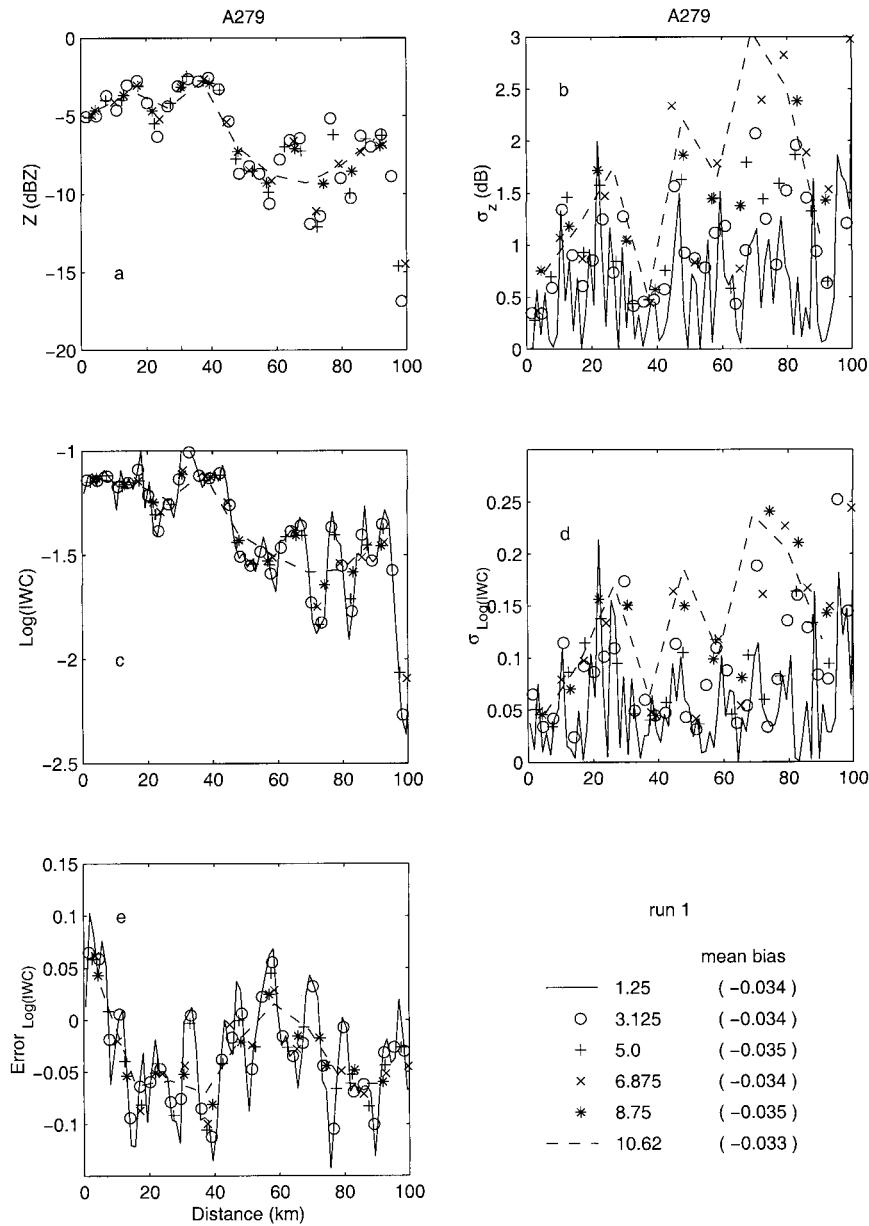


FIG. 13. The effect of different integration distances (km) on the estimates of Z and IWC for one CEPEX aircraft run. (a) Mean Z values; (b) the standard deviation of Z over the integration distance compared with the value from the individual spectra; (c) mean IWC values. (d) As for (b) but the standard deviation of IWC. (e) Fractional error in IWC derived from the averaged Z compared with IWC calculated from the spectra.

fications. The results show that the integration can introduce a bias, but, at least up to a distance of 10.62 km, any bias is usually below 10%. This bias is to be expected because the exponent  $b$  in  $IWC = aZ^b$  is not unity. An analysis of the cumulative frequency shows that for 90% of the time the fraction error in  $\log(IWC)$  due to the integration length over inhomogeneous clouds is less than 0.1, or 25%. If these fractional errors are

plotted as a function of temperature no particular trend is evident.

### 6. Conclusions

In this paper, the accuracy with which IWC can be retrieved from Z has been investigated, and the improvement when either  $D^*$  or  $T$  is available has been

quantified. It has been established that some of the inconsistencies in the published mean relationships between IWC and  $Z$  are due to different assumptions of ice particle density and radar wavelength. Once a common ice density and frequency (94 GHz) are used, then the relationships derived from different datasets in different geographical areas are in agreement to within 20%–30%. However, individual values of IWC derived from specific measurements of  $Z$  are likely to have an error generally in the range +100%/–50%; more specifically, for  $Z$  in the range 0 to –10 dBZ these errors will be about a factor 0.6, but for  $Z$  –20 to –30 dBZ the factor will be about 2.5. There is some uncertainty as to the true variation of density of ice particle with size; this may reduce the value of IWC for a given  $Z$  by 30% and 20%, respectively, when the IWC values are 0.1 and 0.01 g m<sup>–3</sup>. For the lowest temperatures and smallest sizes the probes may be underestimating the IWC, so that for values of IWC < 0.001 g m<sup>–3</sup> the IWC– $Z$  relationship may underestimate the value of IWC. The correct choice of ice density can only be confirmed by extensive comparisons of radar observations and in situ aircraft particle data.

The reduction in the standard deviation of log(IWC) from a  $Z$ – $T$  classification is generally comparable to that from  $Z$ – $D^*$  classification providing the same particle size–density function is used. We find that the standard deviation in log(IWC), which is derived from  $Z$  and  $D^*$ , can fall as low as 0.1 (equivalent to +25%/–20%), but this behavior is restricted to CEPEX tropical data at the high values of  $Z$ . Commonly, for  $Z$  near –15 dBZ, the  $D^*$  classification has an error between 0.15 (+40%/–30%) and 0.2 (+58%/–37%), whereas the  $T$  classification leads to an error of 0.2. For a  $Z$  of –27.5 dBZ the  $D^*$  technique leads to errors of 0.2, as opposed to 0.3 (factor of 2) for the  $T$  method. The minimum standard deviation of 0.1 must be due to the deviations from a pure exponential form; if all spectra were perfectly exponential, then the standard deviation would tend to zero as the breadth of the  $D^*$  category was reduced. For values of  $D^*$  of 35  $\mu\text{m}$  it is advantageous to estimate  $D^*$  to within 5  $\mu\text{m}$ , but once  $D^*$  is above 100  $\mu\text{m}$ , the decreased sensitivity of  $Z$  to  $D^*$  from Mie scattering means that an accuracy of 30% in  $D^*$  is sufficient. This places a lower limit on the required accuracy of the  $D^*$  estimate: a more accurate estimate will not improve the IWC retrievals.

When the mean values of IWC for a given  $Z$  and  $T$  were compared for the two datasets, then the bias was usually less than 25%. An accuracy of  $T$  of 6 K is acceptable; there is no gain if the accuracy is improved to 3 K, and the degradation if 12 K is used is not appreciable. A spaceborne radar may require a horizontal integration length of up to 10 km to achieve a satisfactory sensitivity. The nonlinearity between  $Z$  and IWC may introduce a bias into the retrieved values of IWC from  $Z$  and  $T$ , but for integration lengths of up to 10 km this bias is less than 10%.

The advantage of using the temperature is that it can be derived to within 6 K from a simple numerical forecast model, or in the Tropics, a climatological value may suffice. In contrast deriving  $D^*$  is not trivial; additional lidar measurements can be affected by attenuation, multiple scattering, and crystal shape and density that introduce errors in lidar/radar backscatter ratio.

*Acknowledgments.* This work has been supported by NERC Grant GR3/8765, ESTEC Grant 10568/93 and CEC Grant EV5V CT94-0463. We are grateful to A. J. Heymsfield who provided us with the CEPEX dataset and P. R. A. Brown for the EUCREX dataset.

#### REFERENCES

- Atlas, D., S. Y. Matrosov, A. J. Heymsfield, M. D. Chou, and D. B. Wolff, 1995: Radar and radiation properties of ice clouds. *J. Appl. Meteor.*, **34**, 2329–2345.
- Brown, P. R. A., and P. N. Francis, 1995: Improved measurements of the ice water content in cirrus using a total-water evaporator. *J. Atmos. Oceanic Technol.*, **12**, 410–414.
- , A. J. Illingworth, A. J. Heymsfield, G. M. McFarquhar, K. A. Browning, and M. Gosset, 1995: The role of spaceborne millimetre-wave radar in the global monitoring of ice cloud. *J. Appl. Meteor.*, **34**, 2346–2366.
- Francis, P. N., P. Hignett, and A. Macke, 1998: The retrieval of cirrus cloud properties from aircraft multi-spectral reflectance measurements during EUCREX '93. *Quart. J. Roy. Meteor. Soc.*, **124**, 1273–1291.
- Heymsfield, A. J., and C. M. R. Platt, 1984: A parameterization of the particle size spectrum of ice cloud in terms of ambient temperature and the ice water content. *J. Atmos. Sci.*, **41**, 846–855.
- Hogan, R. J., A. J. Illingworth, and H. Sauvageot, 2000: Measuring ice crystal size in cirrus using 35- and 94-GHz radars. *J. Atmos. Oceanic Technol.*, **17**, 27–37.
- Intrieri, J. M., G. L. Stephens, W. L. Eberhard, and T. Uttal, 1993: A method for determining cirrus cloud particle size using lidar and radar backscatter technique. *J. Appl. Meteor.*, **32**, 1074–1082.
- Knollenberg, R. G., 1970: The optical array: An alternative to scattering for airborne particle size determination. *J. Appl. Meteor.*, **9**, 86–103.
- Kosarev, A. L., and I. P. Mazin, 1991: An empirical model of the physical structure of upper-layer clouds. *Atmos. Res.*, **26**, 213–228.
- Liao, L., and K. Sassen, 1994: Investigation of relationships between Ka-band radar reflectivity and ice and liquid water content. *Atmos. Res.*, **34**, 299–313.
- Locatelli, J. D., and P. V. Hobbs, 1974: Fall speeds and masses of solid precipitation particles. *J. Geophys. Res.*, **79**, 2185–2197.
- Matrosov, S. Y., 1997: Variability of microphysical parameters in high-altitude ice clouds: Results of the remote sensing method. *J. Appl. Meteor.*, **36**, 633–648.
- Maxwell-Garnett, J. C., 1904: Colours in metal glasses and in metallic films. *Philos. Trans. Roy. Soc. London*, **203A**, 385–420.
- McFarquhar, G. M., and A. J. Heymsfield, 1997: Parameterizations of tropical cirrus ice crystal size distributions and implications for radiative transfer: Results from CEPEX. *J. Atmos. Sci.*, **54**, 2187–2200.
- Mitchell, D. L., 1996: Use of mass- and area-dimensional power laws for determining precipitation particle terminal velocities. *J. Atmos. Sci.*, **53**, 1710–1723.
- , R. Zhang, and R. L. Pitter, 1990: Mass-dimensional relationships for ice particles and the influence of riming on snowfall rates. *J. Appl. Meteor.*, **29**, 153–163.

Ou, S.-C., and K.-N. Liou, 1995: Ice microphysics and climate temperature feedback. *Atmos. Res.*, **35**, 127–138.

Sassen, K., 1987: Ice cloud content from radar reflectivity. *J. Climate Appl. Meteor.*, **26**, 1050–1053.

Stephens, G. L., S. C. Tsay, P. W. Stackhouse Jr., and P. J. Flatau, 1990: The relevance of the microphysical and radiative properties of cirrus clouds to climate and climatic feedback. *J. Atmos. Sci.*, **47**, 1742–1753.